


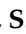






Article

# Optical orientation of excitons in a longitudinal magnetic field in indirect band gap (In,Al)As/AlAs quantum dots with type-I band alignment

T. S. Shamirzaev<sup>1\*</sup> , A. V. Shumilin<sup>2</sup> , D. S. Smirnov<sup>2\*</sup> , D. Kudlacik<sup>3</sup> , S. V. Nekrasov<sup>2</sup> , Yu. G. Kusrayev<sup>2</sup> , D. R. Yakovlev<sup>3,2</sup>  and M. Bayer<sup>3</sup> 

<sup>1</sup> Rzhanov Institute of Semiconductor Physics, Siberian Branch of the Russian Academy of Sciences, 630090 Novosibirsk, Russia

<sup>2</sup> Ioffe Institute, Russian Academy of Sciences, 194021 St.Petersburg, Russia

<sup>3</sup> Experimentelle Physik 2, Technische Universität Dortmund, 44227 Dortmund, Germany

\* Correspondence: sha\_tim@mail.ru and smirnov@mail.ioffe.ru

**Abstract:** The exciton recombination and spin dynamics in (In,Al)As/AlAs quantum dots (QDs) with indirect band gap and type-I band alignment are studied. The negligible (less than 0.2  $\mu\text{eV}$ ) value of the anisotropic exchange interaction in these QDs prevents a mixing of the excitonic basis states with pure spin and allows for the formation of spin polarized bright excitons for quasi-resonant circularly polarized excitation. In a longitudinal magnetic field, the recombination and spin dynamics of the excitons are controlled by the hyperfine interaction between the electron and nuclear spins. A QD blockade by dark excitons is observed in magnetic field eliminating the impact of the nuclear spin fluctuations. A kinetic equation model, which accounts for the population dynamics of the bright and dark exciton states as well as for the spin dynamics, has been developed, which allows for a quantitative description of the experimental data.

**Keywords:** quantum dots; excitons; spins; optical orientation; hyperfine interaction; spin blockade

## 1. Introduction

Spin-dependent phenomena in semiconductor heterostructures are attractive from the viewpoints of both basic physics [1,2] and potential applications [3,4]. Semiconductor quantum dots (QDs) are of great interest as objects with long spin lifetimes of electrons and holes, as the key obstacle for spin-based quantum information processing is spin relaxation. Indeed, the carrier localization slows down the spin relaxation due to suppression of the mechanisms determining the relaxation of freely moving charge carriers [5]. Therefore, the spin relaxation time of electrons localized in QDs can reach milliseconds, as confirmed experimentally [6].

A common approach to study the spin dynamics is optical orientation provided by circularly polarized light [7]. The light delivers angular momentum to the electron spin system, inducing its polarization, which subsequently decays due to relaxation processes. The spin dynamics can be measured by the decay of the photoluminescence (PL) circular polarization degree [7]. However, this technique is not suitable to study the spin dynamics of excitons in direct band gap QDs at zero magnetic field. The axial symmetry breaking, which always occurs in experimentally available QDs, leads to a mixing of the bright pure spin exciton states via the anisotropic exchange interaction [2,8]. Therefore, until recently, optical orientation at zero magnetic field has been used in QDs mainly to study charged excitons (trions) formed, for example, from a pair of electrons and a hole [9]. In this case, the ground state of the trions is an electron spin-singlet for which the exchange interaction with the hole vanishes [10,11].

**Citation:** Lastname, F.; Lastname, F.; Lastname, F. Title. *Nanomaterials* **2023**, *1*, 0. <https://doi.org/>

Received:

Revised:

Accepted:

Published:

**Copyright:** © 2023 by the authors. Submitted to *Nanomaterials* for possible open access publication under the terms and conditions of the Creative Commons Attribution (CC BY) license (<https://creativecommons.org/licenses/by/4.0/>).

We have recently demonstrated the suppression of the anisotropic exchange interaction in indirect band gap (In,Al)As/AlAs QDs, which prevents the bright exciton mixing [12]. Additionally, the weak electron-nuclei interaction in the X valley makes the electrons in such QDs relatively robust against spin decoherence [13]. These features of the exchange and hyperfine interactions allowed for the discovery of the dynamic electron spin polarization effect, which takes place for unpolarized optical excitation in magnetic fields of the order of a few millitesla [14,15]. This effect was later described also for organic semiconductors [16] and moiré QDs [17], where it was recently observed experimentally [18].

In this paper, the exciton recombination and spin dynamics in (In,Al)As/AlAs QDs with indirect band gap and type-I band alignment are studied in a longitudinal magnetic field under optical orientation. The magnetic fields are moderately weak, so that all Zeeman splittings of the spin states are much smaller than the thermal energy. These experimental conditions prevent a circular polarization of the exciton emission to be induced by the magnetic field [19–23]. Measuring the optical orientation in (In,Al)As/AlAs QDs with modulation of the sign of the circular polarization of the exciting light reveals a dependence of the PL circular polarization degree on the modulation frequency, which arises due to the long times of exciton recombination and spin relaxation in indirect gap QDs. Different protocols of the spin orientation measurement are compared, where the effect of QD blockade by dark excitons is found.

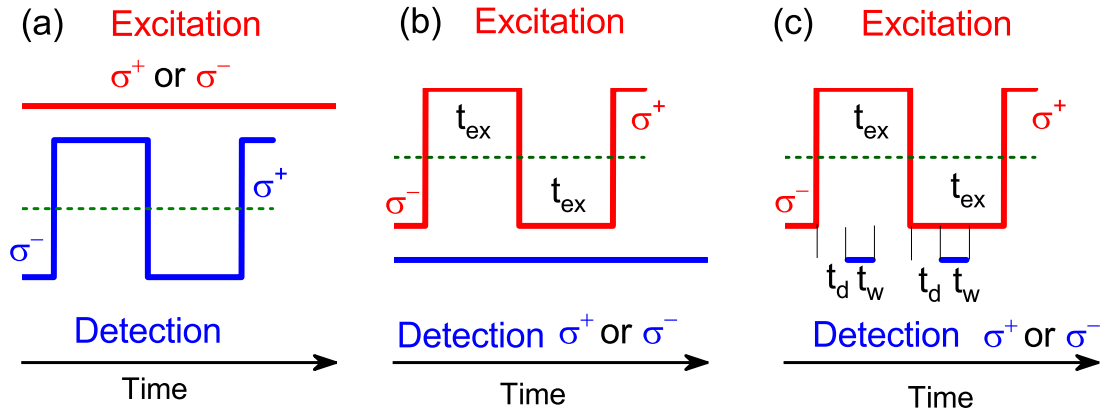
The paper is organized as follows. In Sec. 2 the studied heterostructures and used experimental techniques are described. In Sec. 3 we present the experimental data including time-resolved unpolarized PL, PL under selective excitation in zero magnetic field, the recovery of PL circular polarization in longitudinal magnetic fields for continuous-wave (*cw*) circularly polarized excitation, and the effects of different excitation-detection protocols. Then, in Sec. 4 the theory of exciton spin dynamics in QDs is presented and compared with the experiment.

## 2. Experimental details

The studied self-assembled (In,Al)As QDs embedded in an AlAs matrix were grown by molecular-beam epitaxy on a semi-insulating (001)-oriented GaAs substrate with an 400-nm-thick GaAs buffer layer [24]. The structure contains 20 layers of undoped (In,Al)As/AlAs QDs sandwiched between 25-nm-thick AlAs layers. The nominal amount of deposited InAs is about 2.5 monolayers. Lens-shaped QDs with an average diameter of 15 nm and a height of 4 nm were formed at the temperature of 520°C with the growth interruption time of 20 s. The QD density is about  $3 \times 10^{10} \text{ cm}^{-2}$  in each layer. A 20-nm-thick GaAs cap layer protects the top AlAs barrier against oxidation. Further growth details are given in Ref. [24]. The interlayer distance and QD density were chosen to prevent an electronic coupling between individual quantum dots [25,26]. The growth axis  $z$  coincides with the (001) crystallographic direction. Note, that the band gap energy of the GaAs substrate is 1.52 eV and that of the AlAs barrier is 2.30 eV [27].

The sample was mounted strain free inside a cryostat with a variable temperature insert. The temperature was varied from  $T = 1.7 \text{ K}$  up to 20 K. Magnetic fields in the mT range were generated by an electromagnet with an accuracy better than 0.1 mT. The magnetic field direction coincided with the structure growth axis ( $z$ ), along which also the wave vector of the excitation light was pointing (Faraday geometry).

The PL was excited either non-resonantly with the photon energy of a laser exceeding considerably the emission energies in the QD ensemble, or selectively with a laser energy tuned to a value within the inhomogeneously broadened exciton emission band of the QDs. The nonresonant excitation was provided by the third harmonic of a Q-switched Nd:YVO<sub>4</sub> pulsed laser with the photon energy of 3.49 eV, the pulse duration of 5 ns and the repetition rate of 2 kHz. The excitation density was kept below 100 nJ/cm<sup>2</sup> [28]. For selective excitation a *cw*



**Figure 1.** Protocols used for measurement of  $\rho_c$ : (a) *cw* circularly ( $\sigma^+$  or  $\sigma^-$ ) polarized excitation and modulation of polarization in the detection channel. (b) *cw* measurement of the emission in  $\sigma^+$  or  $\sigma^-$  polarization and modulation of polarization in the excitation channel with the period  $2t_{ex}$ . (c) Modulation of polarization in the excitation channel with the period  $2t_{ex}$  and measurement in the time window  $t_w$  with delay  $t_d$  after changing the excitation polarization.

Ti:Sapphire laser with a photon energy tunable in the spectral range from 1.50 to 1.75 eV was used.

For the time-resolved and time-integrated PL measurements we used a gated charge-coupled-device camera synchronized with the laser via an external trigger signal. The time between the pump pulse and the start of the PL recording,  $t_{delay}$ , could be varied from zero up to 1 ms. The duration of PL recording, i.e. the gate window  $t_{gate}$ , could be varied from 1 ns to 500  $\mu$ s. The signal intensity and the time resolution of the setup depend on  $t_{delay}$  and  $t_{gate}$ . The highest time resolution of the detection system is 1 ns.

For measuring the optical orientation (optical alignment) effects, the circular (linear) polarization of the excitation laser and of the PL emission were selected by corresponding combination of circular (linear) polarizers (Glan-Thompson prism) as well as quarter-wave (half-wave) plates. For the optical orientation measurement, the circular polarization degree of the PL induced by circularly-polarized excitation,  $\rho_c$ , is recorded:

$$\rho_c = \frac{I^{+/+} - I^{+/-}}{I^{+/+} + I^{+/-}}. \quad (1)$$

Here  $I^{a/b}$  is the intensity of the  $\sigma^b$ -polarized PL component measured for  $\sigma^a$ -polarized excitation. The labels + and – correspond to right-hand and left-hand circular polarization, respectively. Note that in our experiments the circular polarization degree induced by the external magnetic field is negligible, since the Zeeman splitting of the excitonic states in the applied magnetic field strength range is much smaller than the thermal energy.

In the optical alignment measurement, the linear polarization degree of the *cw* PL ( $\rho_l$ ) induced by linearly polarized excitation is measured. The linear polarization degree is defined as

$$\rho_l = \frac{I^{0/0} - I^{0/90}}{I^{0/0} + I^{0/90}}, \quad (2)$$

where  $I^{a/b}$  are the PL intensities with the superscripts  $a/b$  corresponding to the direction of the excitation/detection linear polarization. The direction “0” is parallel to the [110] crystallographic direction and the direction “90” is parallel to the  $[\bar{1}\bar{1}0]$  direction.

The electron spin dynamics was investigated by measuring the PL polarization degree for optical orientation in longitudinal magnetic fields. In these experiments, the PL was detected by a GaAs photomultiplier combined with a time-correlated photon-counting module. Three protocols were used: (i) *cw* circularly polarized excitation ( $\sigma^+$  or  $\sigma^-$ ) and measurement of  $\rho_c$  using an acousto-optic quarter-wave modulator with modulation frequency  $f_m = \frac{1}{2 \times t_{\text{ex}}} = 50$  kHz, where  $2 \times t_{\text{ex}}$  is the modulation period [Fig. 1(a)]; (ii) modulation of excitation polarization via an electro-optic half-wave modulator before the quarter-wave plate (with  $f_m$  in the range from 1 up to 500 kHz) and *cw* measurement of the emission in  $\sigma^+$  or  $\sigma^-$  polarization [Fig. 1(b)]; and (iii) the same excitation scenario as in protocol (ii) but measurement with a delay  $t_d$  after changing the excitation polarization (from  $\sigma^+$  to  $\sigma^-$  and vice versa) during the time window  $t_w$  [Fig. 1(c)].

### 3. Experimental results

The dispersion of the QD size, shape, and composition within the ensemble leads to the formation of (In,Al)As/AlAs QDs with different band structures [24], as shown in Fig. 2(a). The electron ground state changes from the  $\Gamma$  to the X valley for decreasing dot diameter, while the heavy-hole (hh) ground state remains at the  $\Gamma$  point, see Fig. 3(a). This corresponds to a change from a direct to an indirect band gap in momentum space, while the type-I band alignment is preserved, that is, in both cases, electron and hole are spatially confined within the (In,Al)As QDs [24,28,29].

Recently, we demonstrated that the coexistence of (In,Al)As/AlAs QDs with direct and indirect band gaps within an ensemble results in a spectral dependence of the exciton recombination times. In the momentum-direct QDs, the excitons recombine within a few nanoseconds. On the contrary, the momentum-indirect QDs are characterized by long decay times due to the small exciton oscillator strength [24,28–34]. Here, we use time-resolved PL to select the indirect band gap QDs.

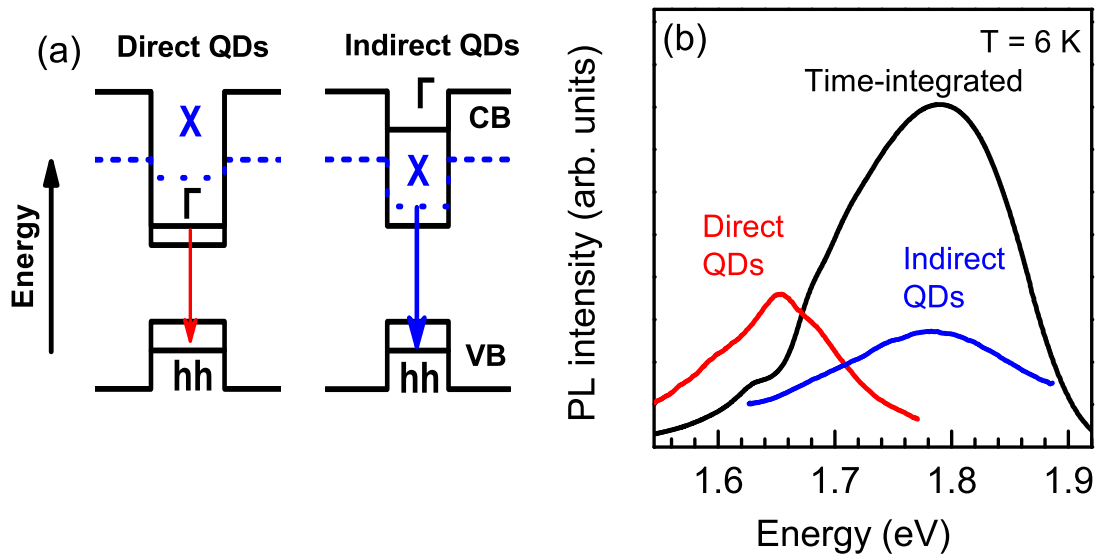
#### 3.1. Time-resolved unpolarized PL

PL spectra of an (In,Al)As/AlAs QD ensemble measured for nonresonant excitation are shown in Fig. 2(b). The time-integrated spectrum (black line) has its maximum at 1.79 eV and extends from 1.5 to 1.9 eV having a full width at half maximum (FWHM) of 190 meV. The large width of the emission band is due to the dispersion of the QD parameters, since the exciton energy depends on the QD size, shape, and composition [24]. The PL band is contributed by the emission of direct and indirect QDs, which becomes evident from the time-resolved PL spectra. When the spectrum is measured immediately after the laser pulse ( $t_{\text{delay}} = 1$  ns and  $t_{\text{gate}} = 4$  ns), the PL band has the maximum at 1.65 eV and the FWHM of 120 meV (red line). For longer delays ( $t_{\text{delay}} = 1000$  ns and  $t_{\text{gate}} = 1500$  ns), the emission maximum shifts to 1.78 eV and broadens to 190 meV (blue line), rather similar to the time-integrated PL spectrum.

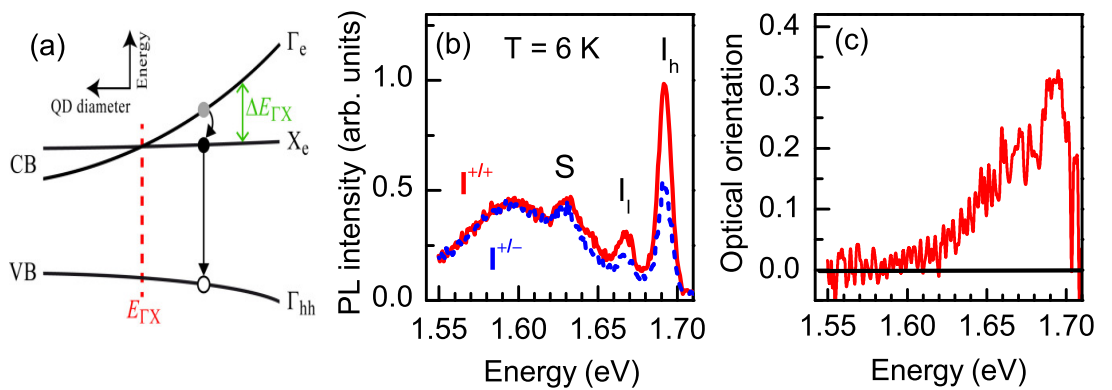
We recently demonstrated that after photoexcitation in the AlAs barriers, electrons and holes are captured into the QDs within several picoseconds, and the capture probability does not depend on the QD size and composition [35]. Therefore, all QDs in the ensemble (direct and indirect ones) become equally populated shortly after the excitation pulse. Thus, the exciton recombination dynamics is fast for direct QDs emitting mainly in the spectral range of 1.50–1.74 eV and slow for the indirect QDs emitting in the range of 1.62–1.90 eV. The emissions of the direct and indirect QDs overlap in the range of 1.62–1.74 eV.

#### 3.2. PL for selective excitation in zero magnetic field

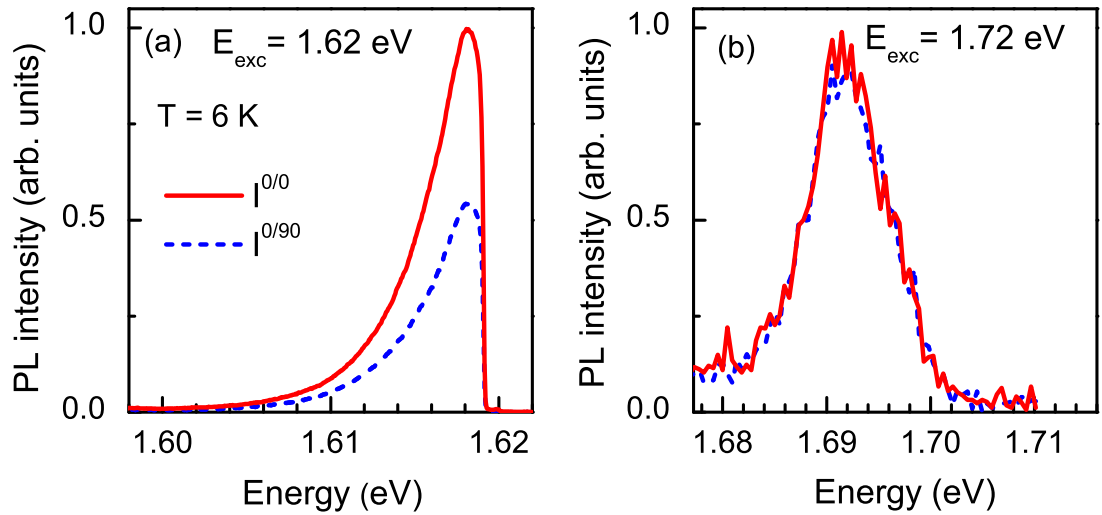
In order to excite only a fraction of QDs with indirect band gap we used selective excitation within the inhomogeneously broadened PL line. As a result, the PL band transforms into a spectrum with rather narrow lines [12]. PL spectra measured for  $\sigma^+$  excitation at  $E_{\text{exc}} = 1.72$  eV



**Figure 2.** (a) Band diagrams of (In,Al)As/AlAs QDs with direct and indirect band structures. Arrows mark the optical transitions related to the decay of the ground state exciton. (b) PL spectra of (In,Al)As/AlAs QDs measured for nonresonant excitation: time-integrated (black line), time-resolved for  $t_{\text{delay}} = 1$  ns and  $t_{\text{gate}} = 4$  ns (red) and for  $t_{\text{delay}} = 1000$  ns and  $t_{\text{gate}} = 1500$  ns (blue).  $T = 6$  K.



**Figure 3.** (a) Band alignment in QDs as function of dot diameter for the valence (VB) and conduction (CB) bands. The energy relaxation of a photo-excited electron from  $\Gamma$  to X, and the subsequent recombination are shown by the arrows. (b) PL spectra of (In,Al)As/AlAs QDs measured in  $\sigma^+$  and  $\sigma^-$  polarization for  $\sigma^+$  circularly polarized excitation,  $E_{\text{exc}} = 1.72$  eV,  $T = 6$  K. (c) Optical orientation calculated from the data shown in panel (b).

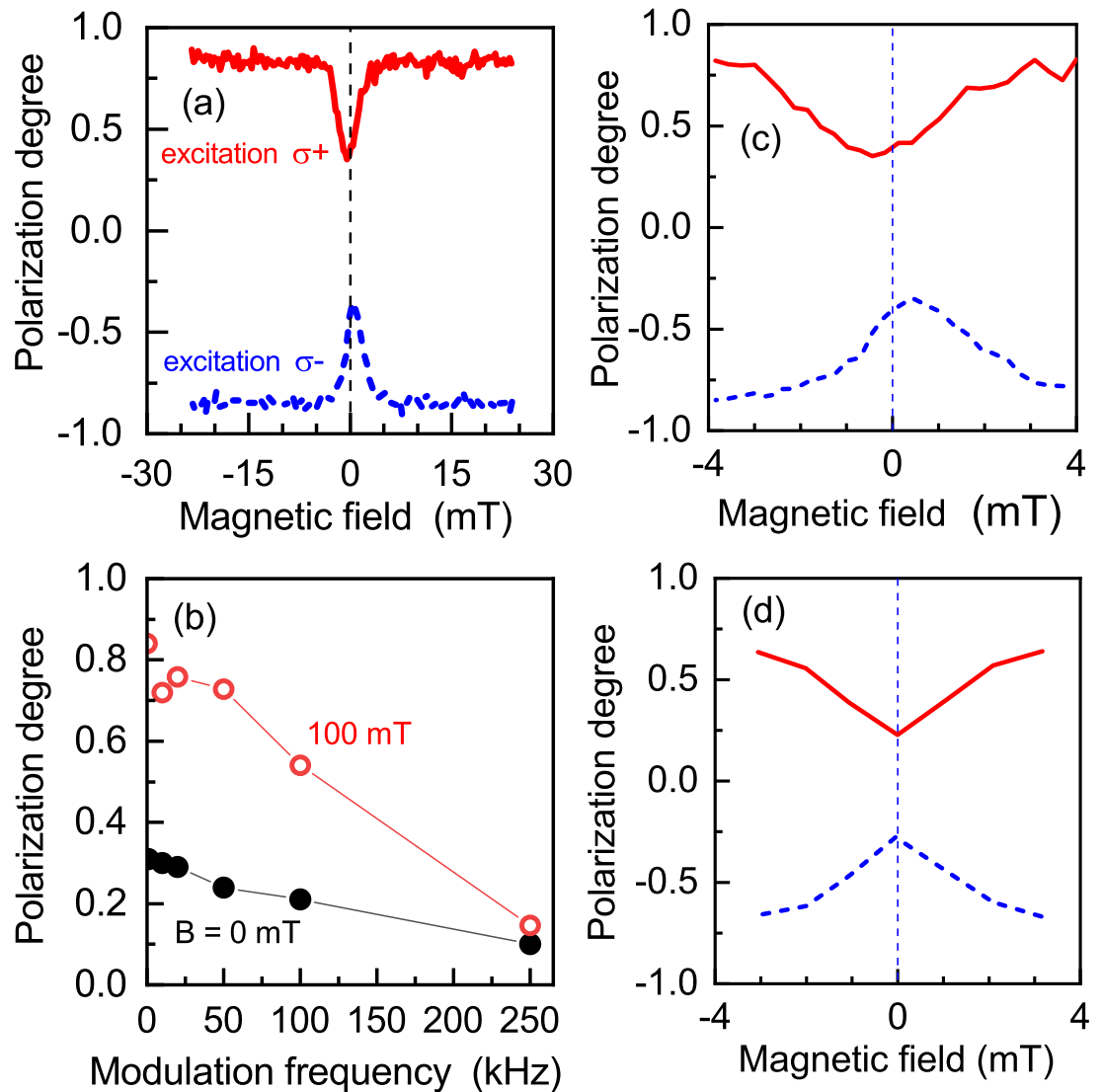


**Figure 4.** Linearly polarized PL spectra of (In,Al)As/AlAs QDs measured for linearly polarized excitation,  $T = 6$  K. (a) Direct band gap QDs,  $E_{\text{exc}} = 1.62$  eV. (b) Indirect band gap QDs,  $E_{\text{exc}} = 1.72$  eV.

using co- and cross-polarized detection are shown in Fig. 3(b). As we showed in Ref. [12], the lines marked as  $I_l$  and  $I_h$  arise from exciton recombination in the indirect QDs, while the line  $S$  arises from a transition in QDs with  $\Gamma$ -X mixing of the electron states. Tuning the excitation energy allows us to selectively excite different sub-ensembles of QDs.

Optical orientation across the PL spectrum for excitation at  $E_{\text{exc}} = 1.72$  eV is shown in Fig. 3(c). The PL in the low-energy spectral region, which corresponds to exciton recombination in direct band gap QDs, demonstrates almost zero optical orientation. Contrary to that, the indirect QDs (high-energy spectral region) demonstrate pronounced optical orientation that reaches 0.3 (i.e. 30 %) at the maximum of the  $I_h$  line (at 1.695 eV). Linearly polarized emission for linearly polarized excitation (optical alignment) is observed for direct QDs, but is absent in indirect QDs, as shown in Figs. 4(a) and 4(b), respectively.

These results are explained by the exciton fine structure. The exciton is formed by a heavy hole with angular momentum projection  $j_z = 3/2$  and an electron with  $s = 1/2$  spin. Accordingly, there are four exciton fine structure states. The two bright exciton states are characterized by the angular momentum projections  $J_z = \pm 1$  onto the growth axis  $z$  and the two dark states have the projections  $J_z = \pm 2$ . The breaking of the axial symmetry in direct QDs lifts the degeneracy of the bright exciton states and mixes them so that the following states emerge:  $|X\rangle = \frac{1}{\sqrt{2}}(|+1\rangle + |-1\rangle)$  and  $|Y\rangle = \frac{1}{i\sqrt{2}}(|+1\rangle - |-1\rangle)$  [36]. A circularly polarized photon excites a superposition of the states  $|X\rangle$  and  $|Y\rangle$ , whose coherence is rapidly lost, destroying the optical orientation of the excitons [37]. Linearly polarized photons, by contrast, excite the pure states  $|X\rangle$  and  $|Y\rangle$  of the bright exciton, so that the linear polarization degree of the emission (optical alignment) is determined by the ratio of the exciton spin decoherence time to the exciton lifetime  $\tau_R$ . The high value of optical alignment for the direct QDs of more than 30% leads us to the conclusion that the spin decoherence time exceeds the recombination one, which is typical for direct band gap QDs [37]. For indirect band gap QDs, the anisotropic electron-hole exchange interaction is negligible due to the weak overlap of the wave functions of the X-electron and the  $\Gamma$ -hole in momentum space [38,39], so that the pure exciton spin states  $J_z = \pm 1$  provide circularly polarized PL [12].



**Figure 5.** (a) Optical orientation in the indirect band gap QDs at 1.695 eV for  $E_{\text{exc}} = 1.72$  eV at  $T = 6$  K. Excitation with protocol (i):  $\sigma^+$  (red solid line) and  $\sigma^-$  (blue dashed line). (b)  $\rho_c^0$  (black circles) and  $\rho_{\text{sat}}$  for  $B = 100$  mT (red circles) as functions of the excitation polarization modulation frequency in protocol (ii). (c) and (d) Details of the PL circular polarization degree near zero external magnetic field for the protocols (i) and (ii), respectively.



### 3.3. Optical orientation in longitudinal magnetic field

Optical orientation at the  $I_h$  line maximum (1.695 eV) for selective *cw* excitation at  $E_{\text{exc}} = 1.72$  eV in protocol (i) [see Fig. 1(a)] as function of the longitudinal magnetic field is shown in Fig. 5(a). One can see that at zero magnetic field the PL polarization degree  $\rho_c^0 = 0.31$ . Already in magnetic fields of a few mT  $\rho_c(B)$  demonstrates a strong change. The optical orientation gradually increases with increasing magnetic field, and saturates at  $\rho_{\text{sat}}=0.84$ , which is about 3 times larger than  $\rho_c^0$ .

The shape of the polarization recovery curve (PRC) is described by a Lorentz curve  $\rho_c(B) = \rho_c^0 + (\rho_{\text{sat}} - \rho_c^0)/(1 + \Delta_{\text{PRC}}^2/B^2)$  with the half width at half maximum of  $\Delta_{\text{PRC}} = 1.8$  mT. We recently demonstrated that  $\Delta_{\text{PRC}}$  arises from the electron spin precession in the local fields created by the nuclear spin fluctuations [40], which govern the electron spin dynamics in magnetic fields  $B \sim \Delta_{\text{PRC}}$  [12–14].

We can estimate the anisotropic exchange interaction for the indirect excitons as  $\delta_1 < \Delta_{\text{PRC}}\mu_B g_e$  [12], where  $\mu_B$  is the Bohr magneton and  $g_e$  is the electron  $g$ -factor. Using  $g_e = 2$  [41–43], we get  $\delta_1 < 0.2$   $\mu\text{eV}$ , which is indeed several orders of magnitude smaller than the  $\delta_1$  of several hundreds of  $\mu\text{eV}$  observed in direct band gap (In,Al)As/AlAs QDs [8].

The increase of the PL polarization degree in a longitudinal magnetic field by a factor of about 3 (from  $\rho_c^0 = 0.31$  to  $\rho_{\text{sat}} = 0.84$ ) indicates that the electron spin relaxation time  $T_1$  is longer than the indirect exciton recombination time. Indeed, the electron spin in a QD undergoes Larmor precession around the effective frozen nuclear field,  $\mathbf{B}_N$ , induced by the nuclear spin fluctuations. The photogenerated spin-oriented electrons lose 2/3 of their spin polarization during the time  $T_2^* \sim \hbar/(g_e\mu_B\Delta_{\text{PRC}})$ , since  $\mathbf{B}_N$  has no preferential orientation and its direction varies from dot to dot in a QD ensemble. The rest 1/3 of the electron spin polarization is stabilized via the interaction with the nuclear spins pointing along the orientation direction, i.e. the  $z$ -axis [12,13]. The deviation of  $\rho_{\text{sat}}$  from unity is the result of the loss of the electron and hole spin polarizations during energy relaxation via the transition from the  $\Gamma$ - $\Gamma$  exciton to the  $\Gamma$ -X exciton [13]. Note that the loss of electron spin polarization alone cannot describe  $\rho_{\text{sat}} < 1$  because the hole spin uniquely defines the emitted photon polarization.

Taking into account the exciton lifetime in the QDs, we can estimate the lower boundary for the spin relaxation time  $T_1$  of electrons in indirect band gap QDs in a longitudinal magnetic field, which eliminates the effect of the nuclear field on the electron spin dynamics. In order to determine the typical exciton lifetime in QDs, we measured the PL dynamics at the detection energy of 1.695 eV for nonresonant excitation, as shown in Fig. 6(a). The PL dynamics are plotted on a double-logarithmic scale, which is convenient to cover the wide range of scanned times and PL intensities.

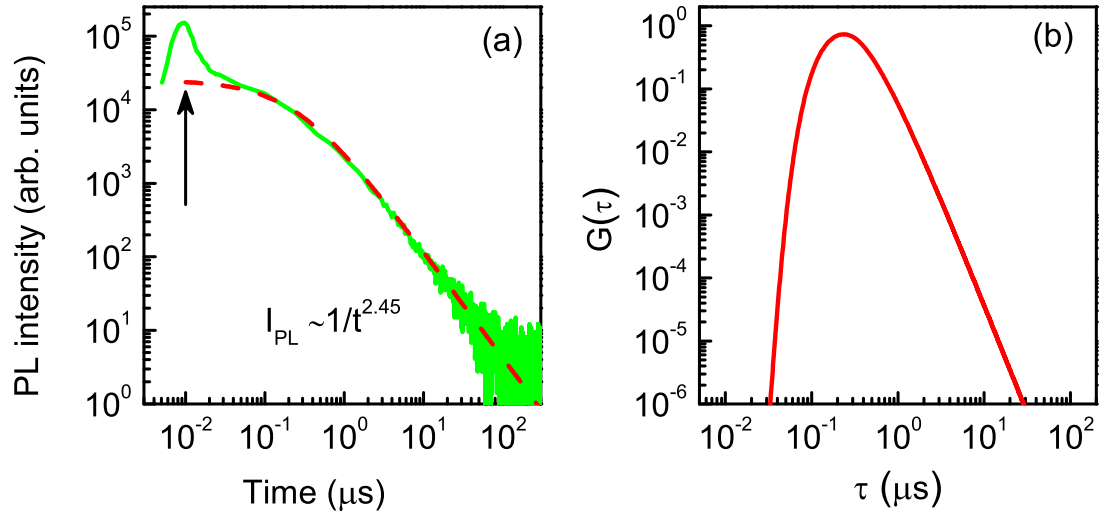
The recombination dynamics demonstrate two distinctive stages: (i) a fast PL decay immediately after the excitation pulse corresponding to recombination in the direct band gap QDs, since direct and indirect QDs are coexisting in this spectral region, see Fig. 2; (ii) a further PL decay that can be described by a power-law function  $I(t) \sim (1/t)^\alpha$ , as shown in our previous studies [24,28,42]. Such a dynamics result from the superposition of multiple monoexponential decays with different times varying with size, shape, and composition of the indirect band gap QDs. It can be described by the following equation [28,44]:

$$I(t) = \int_0^\infty G(\tau) \exp\left(-\frac{t}{\tau}\right) d\tau, \quad (3)$$

where  $G(\tau)$  is the distribution function of the exciton recombination times  $\tau$ . It has the rather simple form [28]:

$$G(\tau) = \frac{C}{\tau^\gamma} \exp\left(-\frac{\tau_0}{\tau}\right). \quad (4)$$





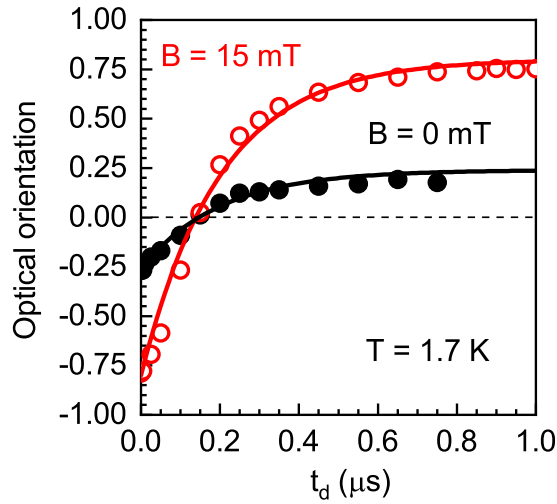
**Figure 6.** (a) PL dynamics measured at the detection energy of 1.695 eV. The excitation pulse with the photon energy of 3.49 eV ends at  $t = 10$  ns (marked by the vertical arrow). The dashed curve is a fit with the parameters given in the text. (b) Normalized exciton lifetime distribution function  $G(\tau)$  corresponding to the QD subensemble emitting at the energy of 1.695 eV, obtained by fitting the PL dynamics.

Here  $C$  is a constant and  $\tau_0$  characterizes the maximum of the distribution of the exciton lifetimes. The parameter  $\gamma$  can be extracted directly from the power-law decay  $(1/t)^{\gamma-1}$  presented in Fig. 6(a). Using the model approach suggested in our recent study [28] we have obtained this distribution function via fitting the recombination dynamics in Fig. 6(a), see the dashed line. The fit parameters are  $\gamma = 3.45$  and  $\tau_0 = 0.25 \mu\text{s}$ . The distribution  $G(\tau)$  is shown in Fig. 6(b). The typical recombination time,  $\tau_0$ , for excitons in the QD subensemble emitting at 1.695 eV equals to  $0.25 \mu\text{s}$ . Thus, the typical spin relaxation time  $T_1$  of electrons in indirect band gap QDs in a longitudinal magnetic field is longer than  $\tau_0 = 0.25 \mu\text{s}$ .

### 3.4. Effect of excitation-detection protocol on the optical orientation

Continuous excitation of localized electrons by circularly polarized light [as we apply in the protocol (i)] can lead via the Knight field to polarization of the nuclear spins, i.e. to dynamic nuclear polarization (DNP) [1,7,45]. The nuclear polarization degree is determined by the ratio between the spin transfer rate from electrons to the nuclei and the nuclear spin relaxation rate [1]. The nuclear spin relaxation times in  $A_3B_5$  semiconductors can reach several seconds, and the Overhauser field of the polarized nuclei acting on the electrons can reach several Tesla [7].

In our case, the DNP manifests itself as a shift of the minimum of the PRC by 0.5 mT from the zero field position, see Fig. 5(c). A change of the excitation polarization (from  $\sigma^+$  to  $\sigma^-$ ) results in a change of the shift direction to the opposite one. Note that the value of the DNP-induced Overhauser field in our indirect band gap QDs is smaller than the typical one (about 10 – 20 mT) observed for direct band gap (In,Ga)As QDs at comparable excitation conditions [46]. The relatively weak DNP-induced Overhauser field in indirect band gap (In,Al)As QDs originates from two specific features of this system: (i) The long exciton lifetime reduces the rate of spin transfer from the electrons to the nuclei. Indeed, the number of electrons that have the possibility to transfer spin polarization to the nuclei in direct band gap systems, which have a typical exciton lifetime of a nanosecond, is about  $10^9$  per second. On the other hand, in systems with indirect band gap, where the exciton lifetime is about a microsecond, this number decreases by several orders of magnitude. (ii) As recently shown, the hyperfine



**Figure 7.** Optical orientation  $\rho_c^0$  (filled black circles) and  $\rho_{\text{sat}}$  for  $B = 15$  mT (open red circles) as functions of the delay time  $t_d$ , measured at  $t_{\text{ex}} = 1$   $\mu\text{s}$  and  $t_w = 0.05$   $\mu\text{s}$ .  $T = 1.7$  K.  $t_d = 0$  corresponds to a change of excitation polarization from  $\sigma^-$  to  $\sigma^+$ . The solid lines show fits after Eq. (5) with the parameters given in the text.

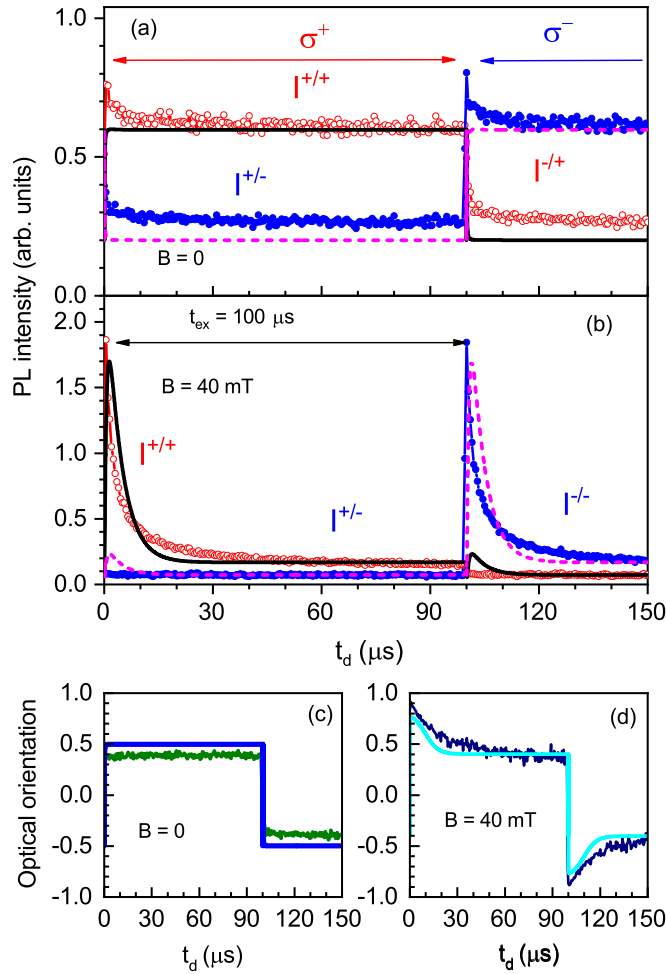
interaction constant for an electron in the X valley of (In,Al)As QDs with the As nuclei is about two times, and with the In and Al nuclei about two orders of magnitude smaller than for an electron in the  $\Gamma$  valley [13]. Thus the Overhauser field induced by polarized nuclei in indirect QDs is several times smaller than the one in direct band gap QDs even at a similar nuclear spin polarization degree.

A common technique for DNP suppression during optical orientation is the modulation of the helicity of the exciting light [7]. We used this technique [excitation corresponding to the protocol (ii)] for the measurement of PRCs. Figure 5(d) demonstrates the absence of a shift of the PRCs at  $f_m = 10$  kHz, which evidences the DNP suppression.

However, a strong difference in optical orientation occurs when using the excitation protocol (ii) compared with protocol (i).  $\rho_c^0$  and  $\rho_{\text{sat}}$  for  $B = 100$  mT are shown in Fig. 5(b) as functions of the modulation frequency of the excitation polarization. One can see that  $\rho_c^0$  decreases with increasing  $f_m$  from 0.31 at  $f_m = 0$  down to 0.10 at  $f_m = 250$  kHz.  $\rho_{\text{sat}}$ , equal to 0.84 at  $f_m = 0$ , decreases down to 0.15 at  $f_m = 250$  kHz.

In order to understand these results, we use the protocol (iii) [see Fig. 1(c)] with different excitation times,  $t_{\text{ex}}$ , delay times,  $t_d$ , and measurement time windows,  $t_w$ . The dependences of  $\rho_c^0(t_d)$  and  $\rho_{\text{sat}}(t_d)$  for  $B = 15$  mT, measured at  $t_{\text{ex}} = 1$   $\mu\text{s}$  and  $t_w = 0.05$   $\mu\text{s}$ , are shown in Fig. 7. One can see that both  $\rho_c^0$  and  $\rho_{\text{sat}}$  at zero delay time, corresponding to the change of excitation polarization from  $\sigma^-$  to  $\sigma^+$ , surprisingly are negative (i.e., are dominated by the counter-polarized  $I^{+/-}$  PL component) and equal to  $-0.75$  ( $-0.25$ ) for  $\rho_{\text{sat}}$  ( $\rho_c^0$ ). When the delay time increases, the optical orientation decreases to zero at  $t_d = 0.15$   $\mu\text{s}$ . A further increase in  $t_d$  changes the polarization to positive values (dominated by the co-polarized  $I^{+/+}$  PL component) and the polarization degree increases to  $+0.75$  ( $+0.25$ ) for  $\rho_{\text{sat}}$  ( $\rho_c^0$ ) at  $t_d = 1$   $\mu\text{s}$ .

The change of the excitation polarization upon modulation of the exciting light in protocols (ii) and (iii) occurs on much shorter timescales than the indirect exciton lifetime. This results in a situation, where after the change of excitation polarization, a fraction of the QDs is still occupied by excitons created in the previous half period of excitation with the corresponding direction of spin polarization, while the other fraction of them begins to become occupied with excitons of opposite spin polarization. Both types of excitons recombine simultaneously emitting oppositely polarized photons. The ratio of oppositely polarized exciton concentrations



**Figure 8.** Intensities of the PL components labeled in the figure as functions of the delay time  $t_d$  for (a)  $B = 0$  mT, and (b)  $B = 40$  mT, measured at  $t_{\text{ex}} = 100$   $\mu\text{s}$  and  $t_w = 2$   $\mu\text{s}$ .  $T = 1.7$  K. The optical orientation corresponding to these functions are presented in panels (c) for  $B = 0$  mT and (d) for  $B = 40$  mT. The theoretical simulations with the parameters given in the text are shown by the solid and dashed lines for the corresponding external magnetic fields.

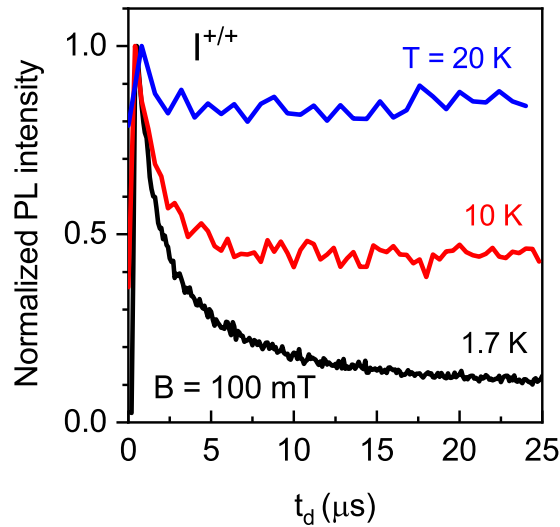
changes with time. Using continuous detection, we measure the integral from all of these processes, which varies with the modulation frequency of the excitation polarization (see Fig. 5(b)).

We describe the dependence of the optical orientation on the delay after changing the excitation polarization as follows:

$$\rho_c(t) = \frac{[I^{+/+}(t) + I^{-/+}(t)] - [I^{+/-}(t) + I^{-/-}(t)]}{[I^{+/+}(t) + I^{-/+}(t)] + [I^{+/-}(t) + I^{-/-}(t)]} = \rho_c^e [1 - 2 \exp(-t/\tau)], \quad (5)$$

where  $\rho_c^e$  is the circular polarization degree at the end of the excitation period for  $t = t_{\text{ex}}$ . One can see that the experimental data in Fig. 7 can be well fitted by Eq. (5) with the exciton recombination time  $\tau = 0.21$   $\mu\text{s}$ , which is in reasonable agreement with the  $\tau_0 = 0.25$   $\mu\text{s}$  obtained from the PL dynamics measurements in Sec. 3.3.

In order to study the spin dynamics at time scales that strongly exceed the exciton lifetimes, we measured the intensities of the co- ( $I^{+/+}$ ) and counter- ( $I^{+/-}$ ) polarized PL components for



**Figure 9.** Intensity of the co-polarized ( $I^{+/+}$ ) PL component as function of the delay time  $t_d$  for  $B = 100$  mT, measured at  $t_{\text{ex}} = 25$   $\mu\text{s}$ ,  $t_w = 2$   $\mu\text{s}$ , and different temperatures.

$t_{\text{ex}} = 100$   $\mu\text{s}$  and  $t_w = 2$   $\mu\text{s}$ . The results of these measurements at zero magnetic field and in an magnetic field of 40 mT (which corresponds to  $\rho_{\text{sat}}$ ) are shown in Fig. 8 as functions of  $t_d$ . At zero magnetic field, both co- and counter-polarized PL component intensities after a short transient process, which follows the change of the excitation polarization, have identical temporal dependences [see Fig. 8(a)], resulting in a constant polarization [see Fig. 8(c)]. However, these dependences change drastically in magnetic field. The intensity of the counter-polarized PL component does not depend on delay time, while the co-polarized PL component increases strongly with the change of excitation polarization, namely by an order of magnitude in Fig. 8(b), and then decays with increasing  $t_d$ . Thus, the PL polarization degree follows the intensity of the co-polarized component [see Fig. 8(d)].

Finally, Fig. 9 shows that at higher temperatures the decay of the co-polarized PL ( $I^{+/+}$ ) with the delay time  $t_d$  becomes weaker.

In conclusion of this section, we summarize the most important experimental findings. The magnetic field dependence of the optical orientation in (In,Al)As/AlAs QDs is changing strongly with the measurement protocol:

(i) The optical orientation depends on the modulation frequency of the excitation polarization.

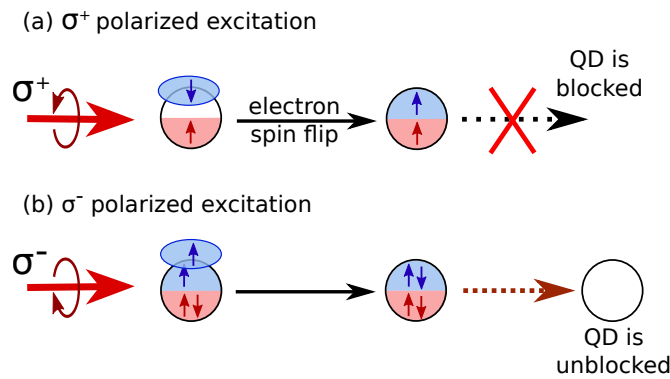
(ii) Measurement of the  $\sigma^+$  and  $\sigma^-$  polarized PL components in a short time window  $t_w$  with delay  $t_d$  after changing the excitation polarization (from  $\sigma^+$  to  $\sigma^-$  and vice versa) allows us to reveal the lifetime and other features of the exciton spin dynamics in indirect QDs.

(iii) At zero magnetic field, both the co- and counter-polarized PL component intensities have identical time dependences, while in a magnetic field with a strength exceeding the fluctuations of the nuclear field, the intensity of the co-polarized PL component increases strongly with changing the excitation polarization and then decays with increasing  $t_d$ . However, the intensity of the counter-polarized PL component does not depend on the delay time.

(iv) The decrease of the co-polarized PL component intensity with delay time  $t_d$  in magnetic field disappears with increasing temperature.

#### 4. Discussion

The most surprising experimental result is shown in Fig. 8. Figure 8(b) evidences that after switching the excitation polarization, the intensity of the co-polarized emission,  $I^{+/+}$  or



**Figure 10.** Blocking of QD due to dark exciton creation (a) and its unblocking after change of the excitation polarization (b).

$I^{-/-}$ , changes strongly at  $t_d \sim 10 \mu s$ . This happens in a magnetic field of 40 mT, while at zero magnetic field there are no such changes, as demonstrated in Fig. 8(a).

In some systems, the decrease of the PL intensity may be related to the suppression of the mixing of dark with bright excitons [17,47] after DNP. However, in our case, we have shown in Sec. 3.3 that the splitting between the bright and dark excitons is small, so that at least half of the excitons created by quasi-resonant excitation are bright. In this case the suppression of the mixing between bright and dark excitons cannot explain the decrease of the PL intensity by an order of magnitude.

We suggest that the observed effect is related to blockade of the QDs by dark excitons. Let us qualitatively describe the mechanism of decrease of the co-polarized PL intensity with time. In a strong enough longitudinal magnetic field, the nuclei-induced mixing between the bright and dark excitons is negligible. In this case,  $\sigma^+$  excitation creates mostly bright excitons, however, due to electron spin relaxation, dark excitons can be also created. These excitons have long lifetimes that are controlled by the hole spin-flip rate  $\gamma_h$ . While each QD can occupy only a single one, dark excitons can accumulate in the ensemble and occupy a significant fraction of the QDs, leading to suppression of the PL intensity [Fig. 10(a)].

When the excitation polarization is switched from  $\sigma^+$  to  $\sigma^-$ , the possibility appears for QDs to capture a second photon and form a biexciton. Fast biexciton recombination returns the blocked QDs to an optically active state, so that the PL intensity recovers [Fig. 10(b)]. The Pauli exclusion principle forbids the biexciton formation for the initial excitation polarization.

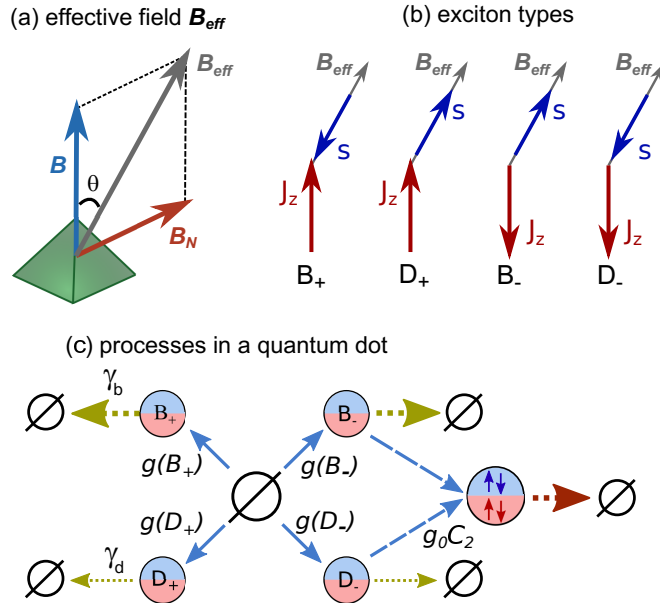
This phenomenon occurs when the applied magnetic fields are strong enough. In zero magnetic field, the bright and dark excitons become in effect mixed by the random nuclear field, so that all of the four exciton types can recombine radiatively quickly. As a result, the PL intensity does not change strongly with time as shown in Fig. 8(a).

With increasing temperature, the electron spin relaxation accelerates, so that the effect of the PL intensity decrease with time disappears, in agreement with Fig. 9.

#### 4.1. Theory of QD blockade

In this section we give a detailed model of the QD blockade by the dark excitons.

For quasi-resonant excitation by  $\sigma^+$  ( $\sigma^-$ ) polarized light, the bright excitons are created in the QDs with a spin-up (-down) heavy hole and a spin-down (-up) electron. We assume that shortly after excitation, electron and hole can flip their spins with the probabilities  $f_e$  and  $f_h$ , respectively, during the exciton relaxation. As a result, the occupancies of the electron spin-up and spin-down states are  $f_e (1 - f_e)$  and  $1 - f_e (f_e)$ , and similarly for the hole spin states. The spin flips may be related to the electron-hole exchange interaction in the direct momentum exciton state or to the electron-phonon interaction during the electron energy relaxation. For



**Figure 11.** (a) Total effective magnetic field  $\mathbf{B}_{\text{eff}}$  acting on an electron, which is composed of the random nuclear field  $\mathbf{B}_N$  and the external field  $\mathbf{B}$  parallel to the growth axis  $z$ . (b) The four exciton eigenstates with the electron spin (blue arrow) along or opposite to the effective magnetic field (grey arrow) and the hole spin (red arrow) along or opposite to the  $z$  axis. (c) Possible transitions between QD states during  $\sigma^+$  excitation,  $\emptyset$  denotes the empty QD state.

the ground state, we describe the electron spin dynamics by the precession in the effective magnetic field  $\mathbf{B}_{\text{eff}}$  composed of the external field  $\mathbf{B}$  and the random nuclear field  $\mathbf{B}_N$  [14,15], see Fig. 11(a). We assume the nuclear field to be quasi-static and Gaussian distributed as  $\propto \exp(-B_N^2/\Delta_B^2)$  [2,40,48], neglecting the anisotropy of the hyperfine interaction [13] and the intervalley hyperfine interaction [49]. Due to the light polarization modulation, a DNP is absent [50], so we neglect it as well as the nuclear spin dynamics, which in principle can take place on a submillisecond time scale [51].

We assume the electron spin precession (the typical period is of the order of 10 ns) to be faster than the exciton recombination, so the direction of  $\mathbf{B}_{\text{eff}}$  defines the appropriate quantization axis for the electron spin. We denote the exciton states with the electron spin along or opposite to the direction of  $\mathbf{B}_{\text{eff}}$  and the hole spin-up or -down as  $B_{\pm}$  and  $D_{\pm}$ , respectively, see Fig. 11(b). In a strong longitudinal magnetic field,  $B_z \gg B_N$ , the effective magnetic field is almost parallel to the  $z$  axis, so  $B_{\pm}$  and  $D_{\pm}$  are quasi-bright and quasi-dark states, respectively.

As described above, we consider the generation of all four exciton states starting from an empty QD. Under  $\sigma^+$  excitation the corresponding generation rates have the form

$$g(B_+) = g_0 \left[ (1-f_h)(1-f_e) \frac{1+\cos\theta}{2} + (1-f_h)f_e \frac{1-\cos\theta}{2} \right], \quad (6)$$

$$g(D_+) = g_0 \left[ (1-f_h)f_e \frac{1+\cos\theta}{2} + (1-f_h)(1-f_e) \frac{1-\cos\theta}{2} \right], \quad (7)$$

$$g(B_-) = g_0 \left[ f_h f_e \frac{1+\cos\theta}{2} + f_h(1-f_e) \frac{1-\cos\theta}{2} \right], \quad (8)$$

$$g(D_-) = g_0 \left[ f_h(1-f_e) \frac{1+\cos\theta}{2} + f_h f_e \frac{1-\cos\theta}{2} \right]. \quad (9)$$

Here  $g_0$  is the pumping rate and  $\theta$  is the angle between  $\mathbf{B}_{\text{eff}}$  and the  $z$  axis, see Fig. 11(a). For  $\sigma^-$  excitation, the subscripts of  $D_{\pm}$  and  $B_{\pm}$  should be flipped.

We take into account the radiative recombination of the bright excitons with the rate  $\gamma_r = 1/\tau$ . In analogy with the generation rates, we find the rates of  $B_{\pm}$  and  $D_{\pm}$  exciton recombination as given by

$$\gamma_b = \gamma_r \frac{1 + \cos \theta}{2}, \quad \gamma_d = \gamma_r \frac{1 - \cos \theta}{2}, \quad (10)$$

respectively, see Fig. 11(c). We also consider the possibility of a hole spin flip with the rate  $\gamma_h$ .

In addition to that, we allow for biexciton formation in a QD, as shown in Fig. 11(c). We assume that under  $\sigma^{\pm}$  excitation it can be formed from the  $B_{\mp}$  and  $D_{\mp}$  excitons only with the rate  $g_0 C_2$  due to the Pauli exclusion principle for the heavy hole spin. The biexciton recombination rate is assumed to be higher than all other recombination rates for simplicity, which, however, hardly affects the results. The biexciton resonance in (In,Al)As/AlAs QDs is detuned from the exciton one [24], therefore, biexciton PL is not detected. However, after biexciton recombination, the QD can be excited once again, so that it becomes optically active. Thus, the role of biexciton generation is to facilitate dark exciton recombination and to unblock the QDs after change of the excitation polarization, see Fig. 10.

The kinetic equations for this model read

$$\frac{dn(B_{\pm})}{dt} = g(B_{\pm})n(\emptyset) + \frac{\gamma_h}{2}[n(D_{\mp}) - n(B_{\pm})] - \gamma_b n(B_{\pm}) - g_0 C_2 \frac{1 \mp \sigma}{2} n(B_{\pm}), \quad (11)$$

$$\frac{dn(D_{\pm})}{dt} = g(D_{\pm})n(\emptyset) + \frac{\gamma_h}{2}[n(B_{\mp}) - n(D_{\pm})] - \gamma_d n(D_{\pm}) - g_0 C_2 \frac{1 \mp \sigma}{2} n(D_{\pm}). \quad (12)$$

Here  $n(B_{\pm})$  and  $n(D_{\pm})$  are the occupancies of the corresponding excitonic states, and  $n(\emptyset)$  is the probability for a QD to be unoccupied. Due to the assumption of a fast biexciton recombination rate, it is given by  $n(\emptyset) = 1 - n(B_+) - n(B_-) - n(D_+) - n(D_-)$ .  $\sigma = \pm$  denotes  $\sigma^{\pm}$  polarization of light. The processes described by these kinetic equation are shown in Fig. 11(c) for  $\sigma = +1$ .

The intensities of  $\sigma^{\pm}$  PL are given by

$$I^{\pm} \propto \gamma_r \left\langle \frac{1 + \cos \theta}{2} n(B_{\pm}) + \frac{1 - \cos \theta}{2} n(D_{\pm}) \right\rangle, \quad (13)$$

where the angular brackets denote the averaging over the nuclear field distribution.

#### 4.2. Modeling of experimental results

To describe the experimental data by this model, we numerically calculate the PL intensity and polarization as functions of the delay time  $t_d$  for  $B = 0$  mT and  $B = 40$  mT. The averaging is performed over 100 random realizations of  $\mathbf{B}_N$ . The comparison between the theoretical and experimental results is shown in Fig. 8. The best fit was obtained using the parameters  $g_0 = 2.2 \mu\text{s}^{-1}$ ,  $\gamma_r = 13 \mu\text{s}^{-1}$ ,  $\gamma_h = 0.035 \mu\text{s}^{-1}$ ,  $C_2 = 0.5$ , and  $\Delta_B = 0.33$  mT. Note that the last parameter is not determined reliably, it should be smaller than 40 mT. The spin-flip probabilities are  $f_h = 0.3$  and  $f_e = 0.25$ . One can see, that the agreement between theory and experiment is good.

The most reliably determined parameter is  $\gamma_h$ , because it describes the decrease of the intensity with time in a strong magnetic field. We also note that the obtained value of  $\gamma_r$  agrees in the order of magnitude with the radiative lifetimes determined independently in Secs. 3.3 and 3.4. A specific feature of our model is that even in strong magnetic fields, the hyperfine



interaction plays a role, because it can cause the recombination rate of the quasi-dark excitons to be comparable to the slow hole spin relaxation rate. In principle, there can be also nonradiative recombination and electron spin flips, which have the same effect. Another feature of the model is the absence of the electron hole exchange interaction, which supports the previous suggestion that it is weak [13,14].

## 5. Conclusion

The exciton recombination and spin dynamics in indirect band gap (In,Al)As/AlAs QDs with type-I band alignment have been studied in a longitudinal magnetic field by means of optical orientation. We have demonstrated that the commonly used technique of measuring the optical orientation based on modulation of the excitation polarization with continuous-wave detection gives ambiguous results, which depend on the modulation frequency due to long exciton recombination and spin relaxation times in this system. A technique based on measuring with a delay after change of the excitation polarization has been proposed for overcoming this problem. A QD blockade by dark excitons has been revealed using this technique. The experimental findings have been quantitatively described by a theoretical model accounting for the population dynamics of the bright and dark exciton states as well as biexciton formation in the QDs.

**Author Contributions:** Conceptualization and methodology, T.S.S.; theoretical investigation, D.S.S and A.V.S; investigation S.V.N.; writing software and optimization of the calculation program, A.V.S; software for the experiment, D.K.; funding acquisition, M.B., T.S.S., Yu.G.K. and D.S.S.; writing—original draft preparation T.S.S. and D.S.S.; writing—review and editing D.R.Y., T.S.S., D.S.S., S.V.N., Yu.G.K. and M.B. All authors have read and agreed to the published version of the manuscript.

**Funding:** The work of D.K., D.R.Y. and M.B. was supported by the Deutsche Forschungsgemeinschaft via the project No. 409810106. D.S.S. thanks the Foundation for the Advancement of Theoretical Physics and Mathematics “BASIS.” The development of the analytical theoretical model of QD blockade by D.S.S. was supported by the Russian Science Foundation, grant No. 21-72-10035. All experimental activities by T.S.S. including sample growth, microscopy, investigation of the energy level spectrum, magneto-optical properties as well as exciton recombination and spin dynamics were supported by a grant of the Russian Science Foundation (No. 22-12-00022). Numeric calculations of luminescence polarization and intensity by A.V.S. were supported by a grant of the Russian Science Foundation (No. 22-12-00125).

**Acknowledgments:** We thank [E. L. Ivchenko](#) and [M. O. Nestoklon](#) for fruitful discussions.

**Conflicts of Interest:** The authors declare no conflict of interest. The funders had no role in the design of the study; in the collection, analyses, or interpretation of data; in the writing of the manuscript; or in the decision to publish the results.

## References

1. *Spin Physics in Semiconductors*, ed. M. I. Dyakonov (Springer, Berlin, 2008).
2. M. M. Glazov, *Electron and Nuclear Spin Dynamics in Semiconductor Nanostructures* (Oxford University Press, Oxford, 2018).
3. A. Fert, Nobel Lecture: Origin, development, and future of spintronics, *Rev. Mod. Phys.* **80**, 1517 (2008).
4. S. D. Bader and S. S. P. Parkin, *Spintronics*, *Annu. Rev. Condens. Matter Phys.* **1**, 71 (2010).
5. A. V. Khaetskii and Yu. V. Nazarov, Spin relaxation in semiconductor quantum dots, *Phys. Rev. B* **61**, 12639 (2000).
6. M. Kroutvar, Y. Ducommun, D. Heiss, M. Bichler, D. Schuh, G. Abstreiter, and J. J. Finley, Optically programmable electron spin memory using semiconductor quantum dots, *Nature* **432**, 81 (2004).
7. *Optical Orientation*, eds. F. Meier and B. P. Zakharchenja (North-Holland, Amsterdam, 1984).
8. J. Rautert, M. V. Rakhlin, K. G. Belyaev, T. S. Shamirzaev, A. K. Bakarov, A. A. Toropov, I. S. Mukhin, D. R. Yakovlev, and M. Bayer, Anisotropic exchange splitting of excitons affected by  $\Gamma$ -X mixing in (In,Al)As/AlAs quantum dots: Microphotoluminescence and macrophotoluminescence measurements, *Phys. Rev. B* **100**, 205303 (2019).
9. M. W. Taylor, P. Spencer, and R. Murray, Negative circular polarization as a universal property of quantum dots. *Appl. Phys. Lett.* **106**, 122404 (2015).

10. D. Dunker, T. S. Shamirzaev, J. Debus, D. R. Yakovlev, K. S. Zhuravlev, and M. Bayer, Spin relaxation of negatively charged excitons in (In,Al)As/AlAs quantum dots with indirect band gap and type-I band alignment, *Appl. Phys. Lett.* **101**, 142108 (2012).
11. T. S. Shamirzaev, D. R. Yakovlev, N. E. Kopteva, D. Kudlacik, M. M. Glazov, A. G. Krechetov, A. K. Gutakovskii, and M. Bayer, Spin dynamics of charged excitons in ultrathin (In,Al)(Sb,As)/AlAs and Al(Sb,As)/AlAs quantum wells with an indirect band gap, *Phys. Rev. B* **106**, 075407 (2022).
12. J. Rautert, T. S. Shamirzaev, S. V. Nekrasov, D. R. Yakovlev, P. Klenovský, Yu. G. Kusrayev and M. Bayer, Optical orientation and alignment of excitons in direct and indirect band gap (In,Al)As/AlAs quantum dots with type-I alignment, *Phys. Rev. B* **99**, 195411 (2019).
13. M. S. Kuznetsova, J. Rautert, K. V. Kavokin, D. S. Smirnov, D. R. Yakovlev, A. K. Bakarov, A. K. Gutakovskii, T. S. Shamirzaev, and M. Bayer, Electron-nuclei interaction in the X valley of (In,Al)As/AlAs quantum dots, *Phys. Rev. B* **101**, 075412 (2020).
14. D. S. Smirnov, T. S. Shamirzaev, D. R. Yakovlev, and M. Bayer, Dynamic Polarization of Electron Spins Interacting with Nuclei in Semiconductor Nanostructures, *Phys. Rev. Lett.* **125**, 156801 (2020).
15. T. S. Shamirzaev, A. V. Shumilin, D. S. Smirnov, J. Rautert, D. R. Yakovlev, and M. Bayer, Dynamic polarization of electron spins in indirect band gap (In,Al)As/AlAs quantum dots in a weak magnetic field: Experiment and theory, *Phys. Rev. B* **104**, 115405 (2021).
16. A. V. Shumilin, Dynamic spin polarization in organic semiconductors with intermolecular exchange interaction, *Phys. Rev. B* **105**, 104206 (2022).
17. D. S. Smirnov, Dynamic valley polarization in moiré quantum dots, *Phys. Rev. B* **104**, L241401 (2021).
18. X. Wang, C. Xiao, H. Park, J. Zhu, C. Wang, T. Taniguchi, K. Watanabe, J. Yan, D. Xiao, D. R. Gamelin, W. Yao, and X. Xu, Light-induced ferromagnetism in moiré superlattices, *Nature* **604**, 468 (2022).
19. E. L. Ivchenko, Magnetic circular polarization of exciton photoluminescence, *Phys. Solid State* **60**, 1514 (2018).
20. T. S. Shamirzaev, J. Debus, D. R. Yakovlev, M. M. Glazov, E. L. Ivchenko, and M. Bayer, Dynamics of exciton recombination in strong magnetic fields in ultrathin GaAs/AlAs quantum wells with indirect band gap and type-II band alignment, *Phys. Rev. B* **94**, 045411 (2016).
21. T. S. Shamirzaev, J. Rautert, D. R. Yakovlev, J. Debus, A. Yu. Gornov, M. M. Glazov, E. L. Ivchenko, and M. Bayer, Spin dynamics and magnetic field induced polarization of excitons in ultrathin GaAs/AlAs quantum wells with indirect band gap and type-II band alignment, *Phys. Rev. B* **96**, 035302 (2017).
22. T. S. Shamirzaev, J. Rautert, D. R. Yakovlev, and M. Bayer, Exciton recombination and spin relaxation in strong magnetic fields in ultrathin (In,Al)As/AlAs quantum wells with indirect band gap and type-I band alignment, *Phys. Rev. B* **104**, 045305 (2021).
23. T. S. Shamirzaev, D. R. Yakovlev, A. K. Bakarov, N. E. Kopteva, D. Kudlacik, A. K. Gutakovskii, and M. Bayer, Recombination and spin dynamics of excitons in thin (Ga,Al)(Sb,As)/AlAs quantum wells with an indirect band gap and type-I band alignment, *Phys. Rev. B* **102**, 165423 (2020).
24. T. S. Shamirzaev, A. V. Nenashev, A. K. Gutakovskii, A. K. Kalagin, K. S. Zhuravlev, M. Larsson, and P. O. Holtz, Atomic and energy structure of InAs/AlAs quantum dots, *Phys. Rev. B* **78**, 085323 (2008).
25. T. S. Shamirzaev, A. M. Gilinsky, A. K. Kalagin, A. I. Toropov, A. K. Gutakovskii, and K. S. Zhuravlev, Strong sensitivity of photoluminescence of InAs/AlAs quantum dots to defects: evidence for lateral inter-dot transport, *Semicond. Sci. Technol.* **21**, 527 (2006).
26. T. S. Shamirzaev, D. S. Abramkin, D. V. Dmitriev, A. K. Gutakovskii, Nonradiative energy transfer between vertically coupled indirect and direct bandgap InAs quantum dots, *Appl. Phys. Lett.* **97**, 263102 (2010).
27. I. Vurgaftman, J. R. Meyer, L. R. Ram-Mohan, Band parameters for III-V compound semiconductors and their alloys, *J. Appl. Phys.* **89**, 5815 (2001).
28. T. S. Shamirzaev, J. Debus, D. S. Abramkin, D. Dunker, D. R. Yakovlev, D. V. Dmitriev, A. K. Gutakovskii, L. S. Braginsky, K. S. Zhuravlev, and M. Bayer, Exciton recombination dynamics in an ensemble of (In,Al)As/AlAs quantum dots with indirect band-gap and type-I band alignment, *Phys. Rev. B* **84**, 155318 (2011).
29. T. S. Shamirzaev, A. V. Nenashev, and K. S. Zhuravlev, Coexistence of direct and indirect band structures in arrays of InAs/AlAs quantum dots, *Appl. Phys. Lett.* **92**, 213101 (2008).
30. D. S. Abramkin, M. A. Putyato, S. A. Budenny, A. K. Gutakovskii, B. R. Semyagin, V. V. Preobrazhenskii, O. F. Kolomys, V. V. Strelchuk, and T. S. Shamirzaev, Atomic structure and energy spectrum of Ga(As,P)/GaP heterostructures, *J. Appl. Phys.* **112**, 083713 (2012).
31. T. S. Shamirzaev, Exciton recombination and spin dynamics in indirect-gap quantum wells and quantum dots, *Phys. Solid State* **60**, 1554 (2018).
32. T. S. Shamirzaev, D. S. Abramkin, A. K. Gutakovskii, and M. A. Putyato, Novel self-assembled quantum dots in the GaSb/AlAs Heterosystem, *JETP Lett.* **95**, 534 (2012).
33. D. S. Abramkin, K. M. Rumynin, A. K. Bakarov, D. A. Kolotovkina, A. K. Gutakovskii, and T. S. Shamirzaev, Quantum Dots Formed in InSb/AlAs and AlSb/AlAs Heterostructures, *JETP Lett.* **103**, 692 (2016).
34. T. S. Shamirzaev, D. S. Abramkin, A. K. Gutakovskii, M. A. Putyato, High quality relaxed GaAs quantum dots in GaP matrix, *Appl. Phys. Lett.* **97**, 023108 (2010).

35. T. S. Shamirzaev, D. S. Abramkin, A. V. Nenashev, K. S. Zhuravlev, F. Trojaneck, B. Dzurnak and P. Maly, Carrier dynamics in InAs/AlAs quantum dots: lack in carrier transfer from wetting layer to quantum dots, *Nanotech.* **21**, 155703-7 (2010).
36. M. Bayer, G. Ortner, O. Stern, A. Kuther, A. A. Gorbunov, A. Forchel, P. Hawrylak, S. Fafard, K. Hinzer, T. L. Reinecke, S. N. Walck, J. P. Reithmaier, F. Klopff, and F. Schäfer, Fine structure of neutral and charged excitons in self-assembled In(Ga)As/(Al)GaAs quantum dots, *Phys. Rev. B* **65**, 195315 (2002).
37. M. Paillard, X. Marie, P. Renucci, T. Amand, A. Jbeli, and J. M. Gérard, Spin relaxation quenching in semiconductor quantum dots, *Phys. Rev. Lett.* **86**, 1634 (2001).
38. G. L. Bir and G. E. Pikus, *Symmetry and Strain-Induced Effects in Semiconductors* (Wiley, New York, 1974).
39. G. E. Pikus and G. L. Bir, Exchange interaction in excitons in semiconductors, *Sov. Phys. JETP* **33**, 108 (1971).
40. I. A. Merkulov, Al. L. Efros, and M. Rosen, Electron spin relaxation by nuclei in semiconductor quantum dots, *Phys. Rev. B* **65**, 205309 (2002).
41. J. Debus, T. S. Shamirzaev, D. Dunker, V. F. Sapega, E. L. Ivchenko, D. R. Yakovlev, A. I. Toropov, and M. Bayer, Spin-flip Raman scattering of the  $\Gamma$ -X mixed exciton in indirect band gap (In,Al)As/AlAs quantum dots, *Phys. Rev. B* **90**, 125431 (2014).
42. V. Yu. Ivanov, T. S. Shamirzaev, D. R. Yakovlev, A. K. Gutakovskii, Ł. Owczarczyk, and M. Bayer, Optically detected magnetic resonance of photoexcited electrons in (In,Al)As/AlAs quantum dots with indirect band gap and type-I band alignment, *Phys. Rev. B* **97**, 245306 (2018).
43. V. Yu. Ivanov, D. O. Tolmachev, T. S. Shamirzaev, D. R. Yakovlev, T. Stupinski, and M. Bayer, Optically detected magnetic resonance of indirect excitons in an ensemble of (In,Al,Ga)As/(Al,Ga)As quantum dots, *Phys. Rev. B* **104**, 195306 (2021).
44. I. S. Nikolaev, P. Lodahl, A. F. van Driel, A. F. Koenderink, and W. L. Vos, Strongly nonexponential time-resolved fluorescence of quantum-dot ensembles in three-dimensional photonic crystals, *Phys. Rev. B* **75**, 115302 (2007).
45. B. Urbaszek, X. Marie, T. Amand, O. Krebs, P. Voisin, P. Maletinsky, A. Högele, and A. Imamoglu, Nuclear spin physics in quantum dots: An optical investigation, *Rev. Mod. Phys.* **85**, 79 (2013).
46. M. S. Kuznetsova, K. Flisinski, I. Ya. Gerlovin, M. Yu. Petrov, I. V. Ignatiev, S. Yu. Verbin, D. R. Yakovlev, D. Reuter, A. D. Wieck, and M. Bayer, Nuclear magnetic resonances in (In,Ga)As/GaAs quantum dots studied by resonant optical pumping, *Phys. Rev. B* **89**, 125304 (2014).
47. M. Dyakonov, X. Marie, T. Amand, P. Le Jeune, D. Robart, M. Brousseau, and J. Barrau, Coherent spin dynamics of excitons in quantum wells, *Phys. Rev. B* **56**, 10412 (1997).
48. D. S. Smirnov, V. N. Mantsevich, and M. M. Glazov, Theory of optically detected spin noise in nanosystems, *Phys. Usp.* **64**, 923 (2021).
49. I. D. Avdeev and D. S. Smirnov, Hyperfine interaction in atomically thin transition metal dichalcogenides, *Nanoscale Adv.* **1**, 2624 (2019).
50. E. A. Zhukov, E. Kirstein, D. S. Smirnov, D. R. Yakovlev, M. M. Glazov, D. Reuter, A. D. Wieck, M. Bayer, and A. Greilich, Spin inertia of resident and photoexcited carriers in singly charged quantum dots, *Phys. Rev. B* **98**, 121304(R) (2018).
51. A. V. Shumilin and D. S. Smirnov, Nuclear Spin Dynamics, Noise, Squeezing, and Entanglement in Box Model, *Phys. Rev. Lett.* **126**, 216804 (2021).

**Disclaimer/Publisher's Note:** The statements, opinions and data contained in all publications are solely those of the individual author(s) and contributor(s) and not of MDPI and/or the editor(s). MDPI and/or the editor(s) disclaim responsibility for any injury to people or property resulting from any ideas, methods, instructions or products referred to in the content.